Journal of Fluids and Structures 17 (2003) 525–539

JOURNAL OF FLUIDS AND STRUCTURES

www.elsevier.nl/locate/jnlabr/yjfls

A compact limit-cycle oscillation model of a cantilever conveying fluid

A. Sarkar, M.P. Païdoussis*

Department of Mechanical Engineering, McGill University, 817 Sherbrook Street West, Montreal, Que., Canada H3A 2K6

Received 1 August 2001; accepted 22 October 2002

Abstract

A low-dimensional model for the planar nonlinear dynamics of a fluid-conveying cantilever is constructed using the proper orthogonal decomposition method (PODM) in the post-flutter region. Firstly, the nonlinear partial differential equation (PDE) of motion is converted into a finite set of coupled ordinary differential equations (ODEs) by a Galerkin projection scheme using the cantilever beam modes as a basis. A finite difference method based on Houbolt's scheme is used to obtain the stable solution of the nonlinear ODEs. A complex eigenvalue analysis is also carried out to determine the region of flutter instability with increasing flow velocity. Secondly, an efficient projection basis for the Galerkin scheme is constructed by using PODM for the low-dimensional representation of the original PDE describing the dynamics of the system. The important question regarding the capability of the reduced-order model to capture the principal features of the original system is addressed. Interestingly, the reduced-order basis constructed using PODM at a specific flow velocity can efficiently reproduce the system response at a range of flow rates involving limit-cycle oscillations (LCO) in the proximity of the flutter point. Furthermore, a weighted POD basis is derived subsequently in order to enhance the efficacy of the reduced-order model over a wider range of flow velocity, in the case when the LCO amplitude exhibits considerable variation beyond the flutter velocity.

1. Introduction

The linear dynamics of a cantilevered pipe conveying fluid has been studied extensively as a classical problem of oscillatory instability involving a gyroscopic nonconservative system (Païdoussis, 1970, 1998; Païdoussis and Li, 1993). The system typically displays oscillatory instability, developing flutter by undergoing a Hopf bifurcation resulting in a limit-cycle oscillation (LCO). In contrast, the end-supported pipe, its conservative counterpart, loses instability through divergence, commonly known as *buckling* (Païdoussis, 1998). In order to capture the nonlinear behaviour of the system, Semler et al. (1994) derived a consistent nonlinear equation of motion accounting for the nonlinear stiffness, inertia and damping terms, correct to third order. The theoretical analysis carried out later on this system (Païdoussis and Semler, 1993, 1998; Semler and Païdoussis, 1995) however, was restricted to low-dimensional models only.

In this paper, higher-dimensional nonlinear dynamical models of a fluid-conveying cantilever are studied, using a Galerkin projection scheme with the cantilever beam modes as a basis. This methodology is perhaps appropriately referred to as a "Fourier–Galerkin scheme" when such a basis consists of harmonic functions (Kwasniok, 1997). Here, however, instead of referring to such a method as "cantilever-beam-mode-Galerkin scheme", which is too long-winded, we decided to refer to it as the Fourier–Galerkin scheme, although the cantilever beam functions are not harmonics. The convergence of the solution scheme of the nonlinear partial differential equation (PDE) in relation to the number of

*Corresponding author. Tel.: +1-514-398-6294; fax: +1-514-398-7365.
E-mail address: mary.fiorilli@mcgill.ca (M.P. Païdoussis).

0889-9746/03/$ - see front matter © 2003 Published by Elsevier Science Ltd.
PII: S0889-9746(02)00150-0

terms retained in the truncated series expansion is systematically studied. Subsequently, a reduced model of the original PDE is constructed by the proper orthogonal decomposition method (PODM), using the time series of the displacement response from the Galerkin projection scheme with the beam modes as basis.

The proper orthogonal decomposition (or Karhunen–Loève decomposition) is an optimal expansion scheme to discretize a random process (Loève, 1977). This well-known approach has been successfully applied to obtain low-dimensional models (Sirovich et al., 1990) of turbulent flow (Sirovich, 1987a, b, c; Aubry et al., 1988; Berkooz et al., 1993), chaotic systems (Sirovich and Rodriguez, 1978; Sirovich, 1989), and convection problems (Sirovich and Deane, 1991). Breuer and Sirovich (1991) used PODM to obtain the eigenfunctions of linear systems. Park and Cho (1996), Park and Yim (1998) and Park and Lee (2000) applied this technique in control problems involving distributed parameter systems. In the context of aeroelasticity, the applications of this approach can be found in Dowell et al. (1997), Kim (1998, 2001), Kim and Bussoletti (2001), Kim et al. (2001), Thomas et al. (2001) and Hall et al. (2000). The use of PODM in nonlinear dynamics of the mechanical systems is elucidated in Cusumano and Bai (1993), Kreuzer and Kust (1996), Georgiou et al. (1999), Ma et al. (2000), Ma and Vakakis (2001) and Lenaerts et al. (2001). The deficiencies and further modification of PODM has been discussed in Christensen et al. (2000) and Lin (1995). Sarkar and Ghanem (2001) have applied PODM in reduced-order modelling of the middle-frequency-range vibration of randomly parametered systems. Kwasniok (1997, 2001) constructed an optimal low-dimensional representation of PDEs using principal interaction patterns, which appears to be even superior to the proper orthogonal decomposition method. However, the approach is considerably more cumbersome compared to PODM from the viewpoint of mathematical analysis and numerical implementation. Kwasniok has also pointed out the limiting case when the principal interaction patterns become identical to the proper orthogonal modes.

To the best of the authors' knowledge, the proper orthogonal decomposition technique is used for the first time in this paper to study the nonlinear dynamical behaviour of the nonlinear PDE describing the motion of a cantilever conveying fluid. The flutter and LCO characteristics of the system are investigated using a reduced-order model emerging from PODM. The proper orthogonal modes (POMs) obtained for a specific flow rate are used to constitute a low-dimensional model which reproduces the system behaviour over a range of flow velocities, specifically the LCOs of the system in the vicinity of the flutter point. To improve the accuracy of the reduced model, a weighted PODM is also derived, which can capture the dynamic behaviour by the low-dimensional model for a wider range of flow velocities, especially in cases when the LCO amplitude undergoes considerable variation with flow rate.

2. Mathematical model

The schematic diagram of the cantilever pipe under consideration is shown in Fig. 1. The system consists of a tubular beam of length L, internal cross-sectional area A, mass per unit length m, flexural rigidity EI, coefficient of Kelvin–Voigt damping a, conveying fluid of mass M per unit length, flowing in the pipe with an axial velocity U. The pipe, initially assumed to lie along the x-axis in the direction of gravity, undergoes oscillation $y(s,t)$ in the (x,y) plane, where s is the curvilinear coordinate. The centre-line of the pipe is assumed to be inextensible. Introducing the nondimensional quantities (Semler et al., 1994)

$$\xi=\frac{s}{L},\quad \eta=\frac{y}{L},\quad \tau=\left(\frac{EI}{m+M}\right)^{1/2}\frac{t}{L^2},\quad \alpha=\left(\frac{EI}{m+M}\right)^{1/2}\frac{a}{L^2},\quad u=\left(\frac{M}{EI}\right)^{1/2}UL,\quad \gamma=\frac{m+M}{EI}L^3g,\quad \beta=\frac{M}{m+M} \tag{1}$$

the equation of motion can be expressed in the following nondimensional form:

$$\begin{aligned}&\alpha\dot\eta''''+\eta''''+\ddot\eta+2u\sqrt{\beta}\dot\eta'(1+\eta'^2)+\eta''\left[u^2(1+\eta'^2)+(\dot u\sqrt{\beta}-\gamma)(1-\xi)\left(1+\frac{3}{2}\eta'^2\right)\right]\\&\quad+\gamma\eta'\left(1+\frac{1}{2}\eta'^2\right)+\left(1+\alpha\frac{\partial}{\partial t}\right)\times[\eta''''\eta'^2+4\eta'\eta''\eta'''+\eta''^3]+\eta'\int_0^\xi(\dot\eta'^2+\eta'\ddot\eta')\,\mathrm{d}\xi\\&\quad-\eta''\left[\int_0^\xi\int_0^\xi(\dot\eta'^2+\eta'\ddot\eta')\,\mathrm{d}\xi\,\mathrm{d}\xi+\int_\xi^1\left(\frac{1}{2}\dot u\sqrt{\beta}\eta'^2+2u\sqrt{\beta}\eta'\dot\eta'+u^2\eta'\eta''\right)\right]\mathrm{d}\xi=0.\end{aligned} \tag{2}$$

2.1. Finite-dimensional representation

The response field $\eta(\xi,\tau)$ is generally expanded using a time-independent global basis which is given by a denumerable and complete set of orthogonal functions in the solution space. Such a basis is obtained from the eigenfunctions of a

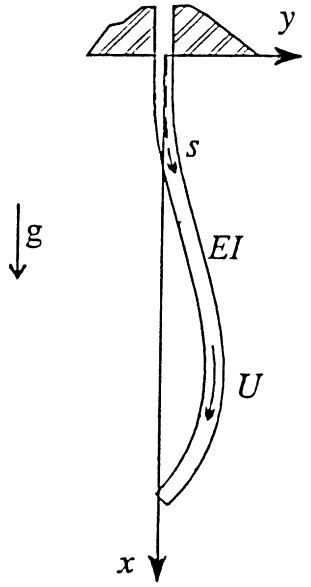

Fig. 1. Schematic diagram of the system.

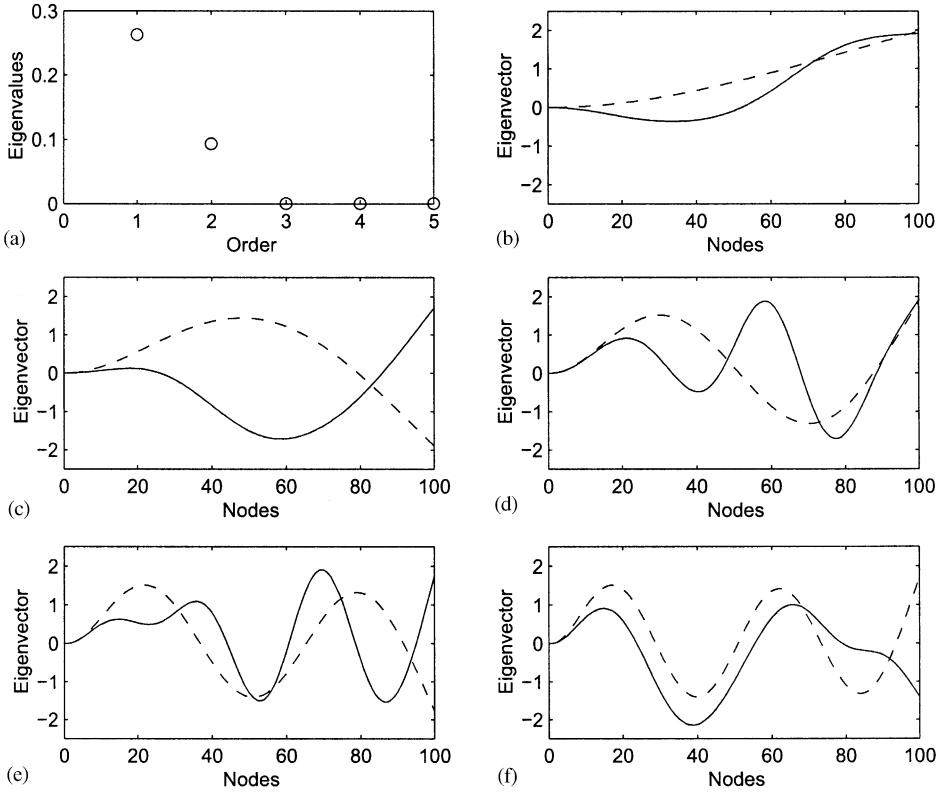

Fig. 2. Eigen-subspace of the correlation matrix for $\gamma = 10$, $\beta = 0.65$ and $u = 13.5$. (a) Eigenvalue spectrum; (b) to (f) eigenvectors of first to fifth modes: —, POM; - - -, corresponding beam mode.

suitably chosen linear self-adjoint differential operator depending on the spatial domain and the boundary conditions. The projection of the nonlinear PDE using the Galerkin approach onto these truncated adjoint-basis functions results in a finite set of coupled nonlinear ODEs which can capture the dynamical characteristics of the PDE with sufficient

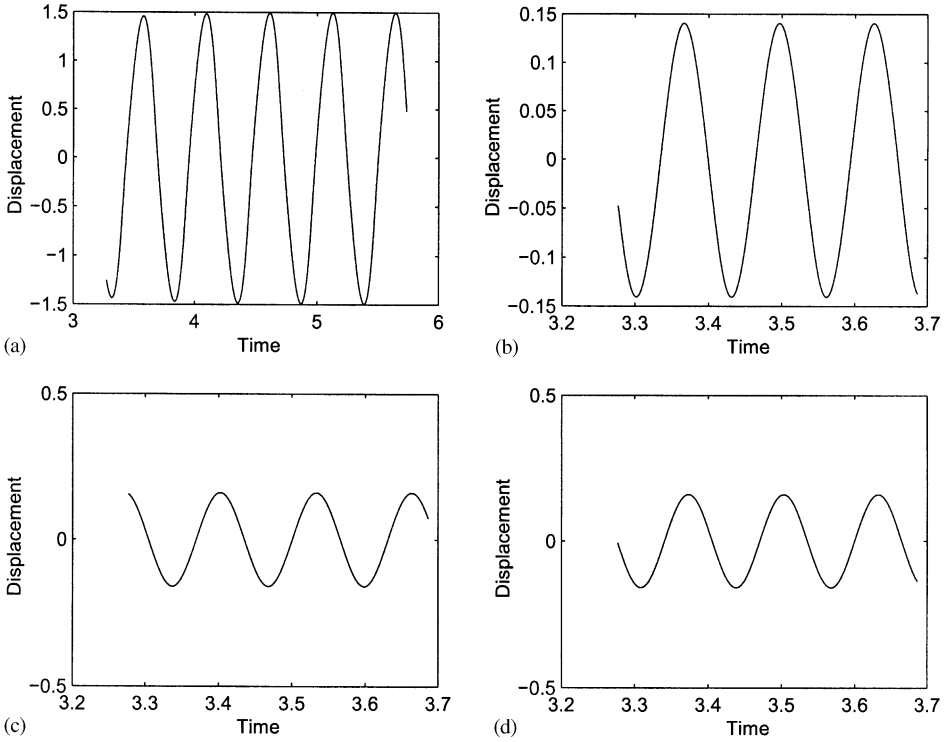

Fig. 3. Time traces using Fourier–Galerkin scheme for $\gamma = 10$, $\beta = 0.65$ and $u = 13.5$: (a) $N = 2$; (b) $N = 6$; (c) $N = 10$. (d) Time trace using POD-Galerkin scheme with $N = 2$.

accuracy. It is worthwhile to point out that the number of degrees of freedom needed in such a Galerkin scheme to reproduce the original system behaviour crucially depends on the appropriate choice of the basis functions. If possible and computationally practicable, the basis functions are taken to be the normal modes of the linear self-adjoint-differential operator corresponding to the original nonlinear PDE. A Galerkin procedure employing any set of such a complete basis functions $\psi_i(\xi)$ approximates the nonlinear PDE (having an infinite number of degrees of freedom) into a finite set of coupled ODEs. However, in many cases, it is not practicable to use the complete linear operator for this purpose, and only a convenient part is used, as discussed in Païdoussis (1998). Indeed, in many cases it is more computationally efficient to use a very simple basis, in which the functions $\psi_i(\xi)$ are known in advance and do not change as parameters are varied. This is the case for the problem at hand, where $\psi_i(\xi)$ are taken to be the linear normal modes of a cantilever beam, in which case the solution of the original PDE in Eq. (2) is expressed as

$$\eta(\xi, \tau) = \sum_{i=1}^{N} \psi_i(\xi) q_i(\tau). \tag{3}$$

Performing Galerkin projections, the coupled ODEs corresponding to Eq. (2) are expressed as

$$\ddot{q}_i + C_{ij}\dot{q}_j + K_{ij}q_j + \alpha_{ijkl}q_j q_k q_l + \beta_{ijkl}q_j q_k \dot{q}_l + \gamma_{ijkl}(q_j \dot{q}_k \dot{q}_l + q_j q_k \ddot{q}_l) = 0. \tag{4}$$

Under the assumption of a steady flow ($\dot{u} = 0$), we obtain

$$C_{ij} = \alpha a_{ij} + 2\sqrt{\beta} u b_{ij}, \tag{5}$$

$$K_{ij} = a_{ij} + (u^2 - \gamma)c_{ij} + \gamma(d_{ij} + b_{ij}), \tag{6}$$

in which

$$a_{ij} = \int_0^1 \psi_i \psi_j'''' \, \mathrm{d}\xi, \quad b_{ij} = \int_0^1 \psi_i \psi_j' \, \mathrm{d}\xi, \quad c_{ij} = \int_0^1 \psi_i \psi_j'' \, \mathrm{d}\xi, \quad d_{ij} = \int_0^1 \xi \psi_i \psi_j'' \, \mathrm{d}\xi \tag{7}$$

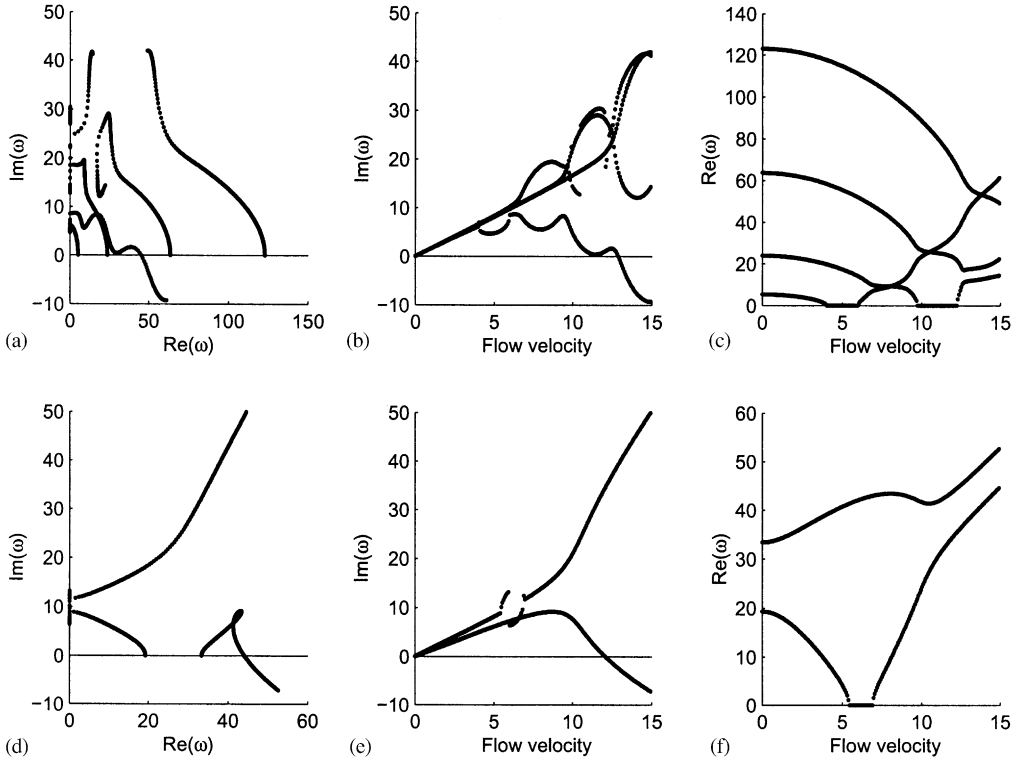

Fig. 4. (a)–(c) The dimensionless complex frequency of the system as function of dimensionless flow velocity, u, for $\gamma = 10$ and $\beta = 0.65$ with Fourier–Galerkin scheme with $N = 10$: (a) Argand diagram (only first four complex frequencies are plotted); (b) imaginary parts of the complex frequencies versus u; (c) real parts of the complex frequencies versus u; the circled numbers in (a) identify the nominal mode number of the locus concerned. (d)–(f) Similar results from the POD-Galerkin scheme ($N = 2$).

and

$$\alpha_{ijkl} = \int_0^1 \psi_i(\psi_j''''\psi_k'\psi_l' + 4\psi_j'\psi_k''\psi_l''' + \psi_j''\psi_k''\psi_l'')\,\mathrm{d}\xi + u^2 \int_0^1 \psi_i\psi_j''\left(\psi_k'\psi_l' - \int_\xi^1 \psi_k'\psi_l''\,\mathrm{d}\xi\right)\mathrm{d}\xi + \gamma \int_0^1 \psi_i\left(\frac{1}{2}\psi_j'\psi_k'\psi_l' - \frac{3}{2}(1-\xi)\psi_j''\psi_k'\psi_l'\right)\mathrm{d}\xi, \tag{8}$$

$$\beta_{ijkl} = 2u\sqrt{\beta}\int_0^1 \psi_i\left(\psi_j'\psi_k'\psi_l' - \psi_j''\int_\xi^1 \psi_k'\psi_l''\,\mathrm{d}\xi\right)\mathrm{d}\xi, \tag{9}$$

$$\gamma_{ijkl} = \int_0^1 \psi_i\psi_j'\left(\int_0^\xi \psi_k'\psi_l'\,\mathrm{d}\xi\right)\mathrm{d}\xi - \int_0^1 \psi_i\psi_j''\left(\int_\xi^1\int_0^\xi \psi_k'\psi_l'\,\mathrm{d}\xi\right)\mathrm{d}\xi. \tag{10}$$

In the first instance, this approach is adopted here to solve the PDE, and convergence of the solution is studied in relation to the number of terms retained in the expansion. For brevity, this methodology will be referred to as *the Fourier–Galerkin scheme* in what follows, as mentioned before.

2.2. Linear stability analysis

The linear stability analysis can be carried out by studying the eigenvalues of the linear version of Eq. (4),

$$\ddot{q}_i + C_{ij}\dot{q}_j + K_{ij}q_j = 0, \tag{11}$$

as the flow velocity is increased. The complex eigenvalues will be presented in the form of Argand diagrams. In such a diagram, the onset of oscillatory instability or *flutter*, as exhibited by this specific system, is identified as the point

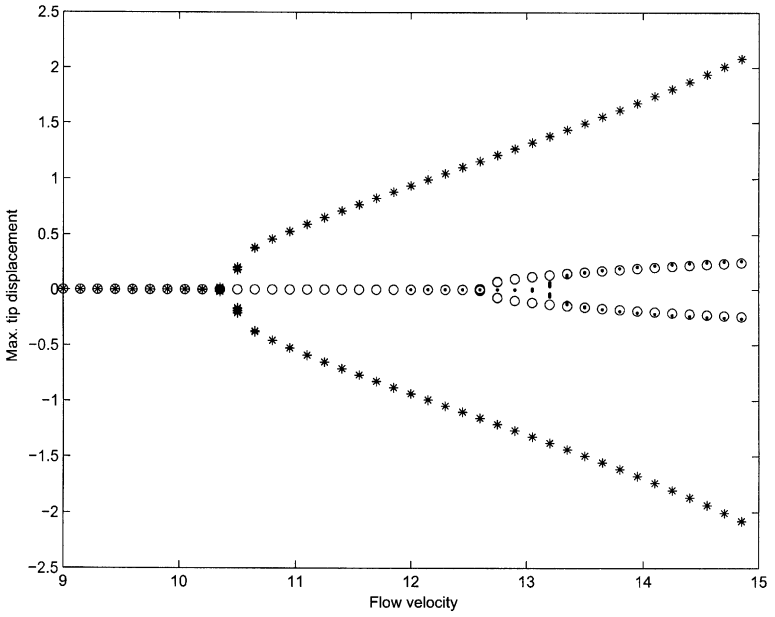

Fig. 5. Bifurcation diagrams for $\gamma = 10$ and $\beta = 0.65$: *, Fourier–Galerkin scheme for $N = 2; \ldots$, same for $N = 10$; and $\circ$, POD-Galerkin scheme for $N = 2$.

when the imaginary part of any one of the eigenfrequencies becomes negative, inducing a negative damping in the system.

3. Proper orthogonal decomposition (PODM)

In numerous contexts, the dynamics of PDEs are often confined to attractor sets of relatively low dimension in the appropriately selected solution coordinates. Despite the popularity and compact mathematical framework of the Fourier–Galerkin schemes, the basis consisting of the normal modes of the linear self-adjoint system corresponding to the nonlinear PDE is very general and does not contain any information regarding the intrinsic nonlinearity existing in the original nonlinear PDE. Thus, the methodology does not adapt well to the particular system at hand. Consequently, such a basis is generally not the best choice in expanding the solution of the nonlinear PDE. In this particular case, where the cantilever beam eigenfunctions are used for $\psi_i(\xi)$, these modes do not even contain any information on the effect of flow, and in the case of vertical pipes ($\gamma \neq 0$), not even on the effect of gravity. Thus, the order of the systems of ODEs obtained using the Fourier–Galerkin approach is much larger than the true dimensionality of the original PDE. It becomes then logical to incorporate the features involving the nonlinearities, flow effects, etc., existing in the original system in order to construct the basis functions, and so arrive at a low-dimensional model reflecting more closely the inherent dimensionality of the original PDE.

In this context, the proper orthogonal decomposition method appears to be an obvious choice. In numerous papers, the dimensionality and spatio-temporal complexities have been successfully studied using the PODM, also known as Karhunen–Loève expansion. The method optimally extracts spatial information and identifies the dimensionality of a system from a set of time-series data gathered from numerical simulations or physical experiments. The model reduction of the system is achieved using two steps. Firstly, the traditional Fourier–Galerkin scheme is used to obtain the converged solution of the original PDE. Secondly, an efficient POD basis is constructed using the system response (obtained from the Fourier–Galerkin scheme), onto which the original PDE is projected to obtain an alternative, better low-dimensional model.

3.1. Direct PODM

Consider a time series $u(x,t)$, sampled at a location x_j, $j = 1 \ldots n$ at time instants t_i, $i = 1 \ldots M$, with uniform time intervals consistent with the Nyquist frequency. The PODM represents the time series $u(x,t)$ with an optimal (in the

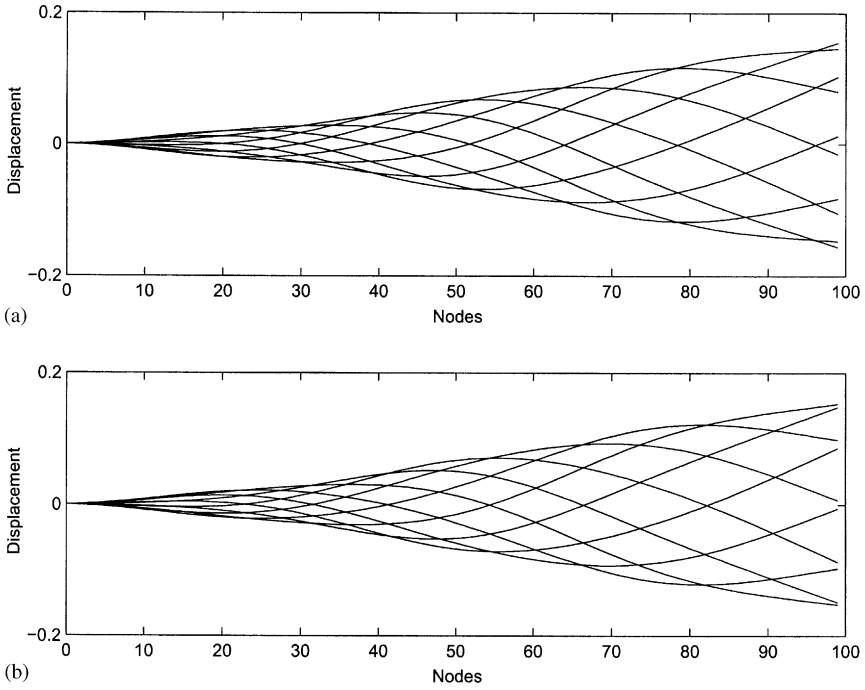

Fig. 6. Temporal snapshots of spatial responses for $\gamma = 10$ and $\beta = 0.65$: (a) Fourier–Galerkin scheme with $N = 10$; (b) POD-Galerkin approach with $N = 2$.

mean-square sense) number of degrees of freedom where the basis vectors are obtained by solving the maximization problem (see, e.g. Sirovich and Deane, 1991; Berkooz et al., 1993; Park and Lee, 2000).

$$\lambda = \frac{\int\int_{\Omega} \langle u(\mathbf{x},t), u(\mathbf{y},t)\rangle \Psi(\mathbf{x})\Psi(\mathbf{y})\,\mathrm{d}\mathbf{x}\,\mathrm{d}\mathbf{y}}{\int_{\Omega} \Psi(\mathbf{x})\Psi(\mathbf{x})\,\mathrm{d}\mathbf{x}}, \tag{12}$$

where $\langle . \rangle$ is the time-averaging operator and Ω is the spatial domain of integration. The optimization problem finally leads to a eigenvalue problem, stated as

$$\boldsymbol{C\Psi} = \lambda \boldsymbol{\Psi}, \tag{13}$$

where the time-averaged two-point correlation matrix is given by

$$C(\mathbf{x},\mathbf{y}) = \frac{1}{M}\sum_{i=1}^{M} u(\mathbf{x},t_i)u(\mathbf{y},t_i), \tag{14}$$

where M is the number of sample points and the set of $\boldsymbol{\Psi}$s are the spatial coherent structures in the spatio-temporal records. The dominant eigensubspace of the eigenvalue problem of the correlation matrix, determines the dominant spatially coherent modes. An eigenvector $\boldsymbol{\Psi}$ is referred to as the coherent fluctuation or proper orthogonal mode (POM), and λ represents the amount of energy captured by the corresponding mode; λ is always positive. The correlation matrix being symmetric and positive-definite, the POMs form a complete orthogonal basis which can represent the process $u(\mathbf{x},t)$. They are also optimal, in the sense that they capture more energy than any other set of basis functions, with a minimum number of terms. The optimal system dimension N is determined as $\sum_{i=1}^{N} \lambda_i / \sum_{i=1}^{n} \lambda_i \geqslant 99\%$, assuming the sufficiency of the POMs to capture 99 percent of the energy of the signal. In relation to the present study, the solution $\eta(\xi,\tau)$ of the PDE given by Eq. (2) will be approximated using the POMs obtained at a specific flow rate as basis. The coherent structures or POMs constructed at a specific flow velocity, however, may not be the coherent structures at any other flow velocity. However, the new coherent structure or POMs can be calculated from the time series of the response obtained using the POMs at a neighbouring flow velocity. Interestingly, as will be demonstrated later, the POMs constructed at a specific flow rate beyond the flutter velocity can

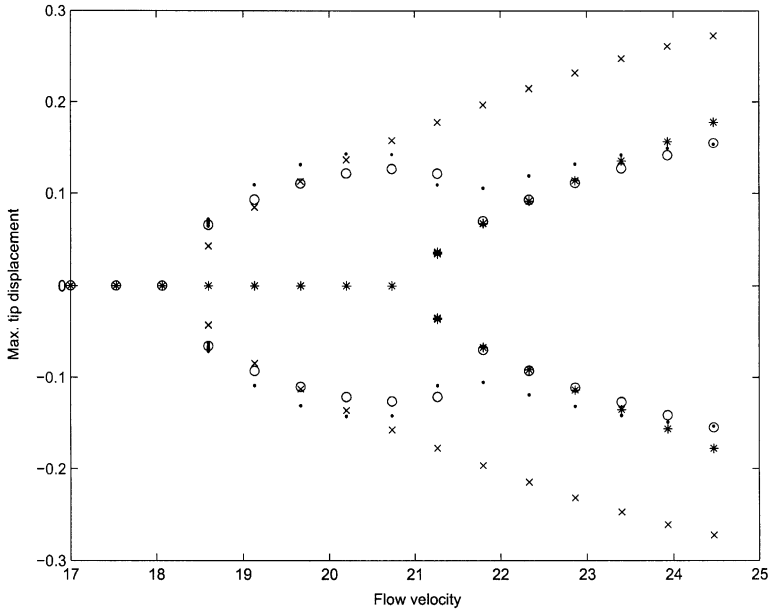

Fig. 7. Bifurcation diagrams for $\gamma = 100$ and $\beta = 0.65$: $\cdot$, for Fourier–Galerkin scheme with $N = 10$; $\times$, for POD-Galerkin scheme from $u = 20$ data and $N = 4$; $*$, for POD-Galerkin scheme from $u = 23$ data and $N = 4$; $\circ$, for *weighted* POD-Galerkin scheme with $N = 4$ for $u_1 = 20$ and $u_2 = 23$ with corresponding weights $w_1 = 0.5$ and $w_2 = 0.5$.

efficiently reproduce the system response with a low-dimensional model for a reasonably wide range of flow velocities involving LCOs. This aspect will be illustrated through numerical examples in Section 4.

3.2. Weighted PODM

Depending on the system parameters, the LCO amplitude can display considerable variation as flow velocity is increased, resulting in a significant change in the POMs. Consequently, the POMs constructed at a specific flow rate may no longer be an efficient projection basis at a neighbouring flow velocity. To circumvent the problem of constructing a new set of POMs at each flow velocity, a weighted PODM is now adopted in this section. This approach allows a single POD basis to devise an efficient solution scheme for the PDE with a cosiderable variation of flow rate. Identification of such weighted POMs can be effectively formulated in terms of a multi-objective optimization problem. The two general approaches to such multicriteria optimization problems are *preference* and *nonpreference* methods. The preference method makes use of the explicit information regarding the relative importance of the different objective criteria in order to identify a best overall solution. The nonpreference method, often referred to as Pareto optimization, makes no such assumption about the relative importance of different objective criteria, but instead, identifies a field of solutions where no solution is classified to be better than any other solution in the field for all objective criteria. The Pareto optimization scheme is specifically suitable for the *nonconvex* optimization problem involving conflicting objectives (Zlobec, 2001). In this paper, we consider the *preference* approach in order to generate the weighted POMs. A conflict between the different objectives to determine the best possible POMs appropriate for all flow rates may emerge, as will be explained later. The preference approach can handle such optimization issue if the problem at hand is *convex* in nature (Pareto, 1906; Koski, 1985; Das and Dennis, 1997; Zlobec, 2001). As will be demonstrated by the results, a remarkable feature of the weighted POD scheme for this specific problem, is that the results are not sensitive to the weights used in the preference approach.

The weighted POMs are obtained by solving the following eigenvalue problem:

$$\left[\sum_{k=1}^{M} w_k \boldsymbol{C}_k\right] \boldsymbol{\Psi} = \lambda \boldsymbol{\Psi}, \tag{15}$$

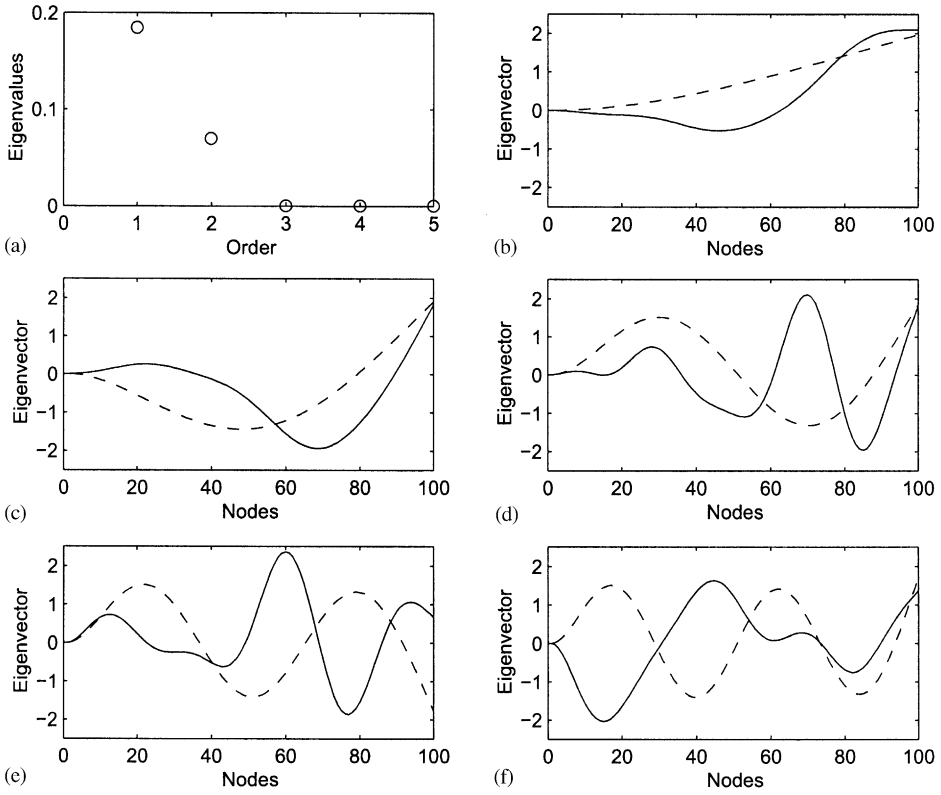

Fig. 8. Eigen-subspace of the correlation matrix for $\gamma = 100$, $\beta = 0.65$ and $u = 20$: (a) eigenvalue spectrum; (b)–(f) eigenvectors of first to fifth modes (—) compared to corresponding beam mode (- - -).

emerging from the maximization problem

$$\lambda = \frac{\int\int_\Omega [\sum_{k=1}^{P} w_k \langle u(\mathbf{x}, t; U_k), u(\mathbf{y}, t; U_k)\rangle] \Psi(\mathbf{x})\Psi(\mathbf{y})\,\mathrm{d}\mathbf{x}\,\mathrm{d}\mathbf{y}}{\int_\Omega \Psi(\mathbf{x})\Psi(\mathbf{x})\,\mathrm{d}\mathbf{x}}, \tag{16}$$

where P is the number of discrete flow velocities at which the time series of the response is obtained, and w_k is the weight given to the response time series constructed at flow velocity U_k. The convexity of the optimization problem can be realized directly from each objective function $\mathscr{H} = \int\int_\Omega \langle u(\mathbf{x}, t; U), u(\mathbf{y}, t; U)\rangle \Psi(\mathbf{x})\Psi(\mathbf{y})\,\mathrm{d}\mathbf{x}\,\mathrm{d}\mathbf{y}$ having positive Hessian function $\partial^2\mathscr{H}/\partial\Psi^2 > 0$. Note that the aforementioned weighted PODM conceptually bears close similarity to the work by Kim (2001) and Kim et al. (2001). It will be shown numerically that the weighted PODM model can efficiently reproduce the response of the complete dynamical system obtained using the Fourier–Galerkin approach.

4. Numerical examples

Based on the aforementioned mathematical formulation, a numerical investigation is carried out in this section. The solutions of the set of nonlinear ODEs are obtained by a finite difference method based on Houbolt's scheme (Semler et al., 1996), with a time-step size of 0.0001. The damping coefficient $\alpha = 0$ is taken to be zero.

In Fig. 2, the eigenvalues and eigenvectors of the correlation matrix in Eq. (13) are plotted for the flow velocity $u = 13.5$ for a fluid-conveying cantilever with $\beta = 0.65$ and $\gamma = 10$. From the eigenvalue spectrum in Fig. 2(a), the order of the reduced model is clearly identified to be 2. Consequently, only the eigenvectors corresponding to these two largest eigenvalues are used as a basis to obtain a convergent solution. In Figs. 2(b)–(f), the solid and dashed lines represent the successive POMs and the beam modes of the linear structure. Evidently, the POMs differ significantly from the beam modes in order to capture both linear and nonlinear characteristics of the system *in flow* with just two modes; in this way, POMs emerge as a superior basis for a reduced-order model.

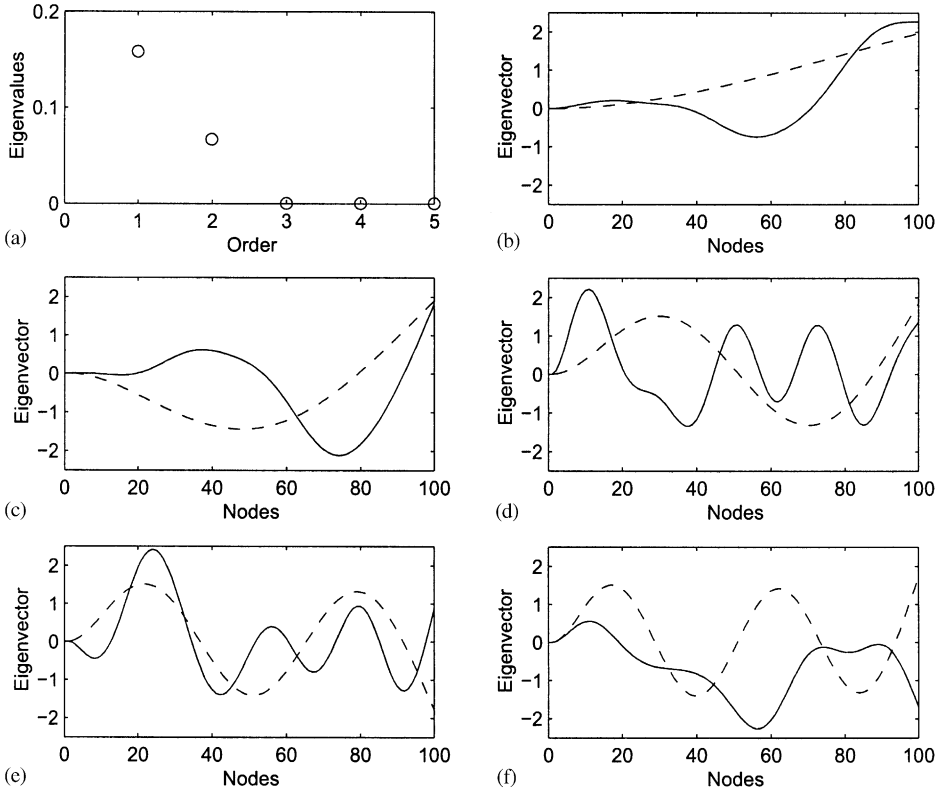

Fig. 9. Eigen-subspace of the correlation matrix for $\gamma = 100$, $\beta = 0.65$ and $u = 23$: (a) eigenvalue spectrum; (b)–(f) eigenvectors of first to fifth modes (—) compared to corresponding beam mode (- - -).

In Fig. 3(a)–(c), the tip displacement responses obtained by using 2-, 6- and 10-dof Fourier–Galerkin schemes are shown, in order to study the convergence of the solution. No significant improvement in the time traces of the response is observed in the Fourier–Galerkin scheme by taking terms higher than 10 in expanding the solution. In Fig. 3(d), the result obtained using 2-dof POD-Galerkin method is presented, which compares well with the result using 10-dof Fourier–Galerkin approach of Fig. 3(c).

The Argand diagram (representing the complex eigenfrequencies of the linear system plotted in terms of their real and imaginary parts as functions of the dimensionless flow velocity u) is presented in Fig. 4(a) obtained using the 10-dof Fourier–Galerkin approach. Only the lowest four eigenfrequencies are plotted for clarity. Note that only one mode, the nominal "first mode" becomes unstable by crossing the real axis, thus resulting in a negative damping in the system. The real and imaginary parts of the complex eigenfrequencies are plotted separately versus the flow velocity in Fig. 4(b) and (c). Similar plots are also shown in Fig. 4(d)–(f) obtained with the 2-dof POD-Galerkin approach, the POMs having been obtained from simulation at $u = 13.5$. From Figs. 4(b) and (e), it is seen that the critical flutter velocity ($u_{cr} \simeq 12.5$) predicted by 2-dof POM-Galerkin approach matches quite well with the result from 10-dof Fourier–Galerkin method ($u_{cr} \simeq 12.75$). However, in the POD case, a mode veering has taken place, and the second part of the first-mode locus at higher u is exchanged with that of the second mode. This is not unusual (Païdoussis, 1998).

Fig. 5 presents the bifurcation diagram constructed using the Fourier–Galerkin method with 2- and 10-dof. The result from the 2-dof POD-Galerkin approach is also plotted, with the POMs obtained from simulations at $u = 13.5$. Interestingly, the 2-dof POD-Galerkin method can efficiently reconstruct the LCO amplitude over a range of flow velocity, whereas the result from 2-dof Fourier–Galerkin model is unacceptably different, as expected; see Païdoussis (1970, 1998).

Fig. 6(a) and (b) shows the snapshots of the spatial response of the cantilever at various time steps obtained by the 10-dof Fourier–Galerkin and 2-dof POD-Galerkin method. The spatial responses obtained using these two methodologies show an excellent match, as expected.

Fig. 7 shows the bifurcation diagram for a system $\beta = 0.65$ and $\gamma = 100$. The bifurcation diagram, constructed using a 10-dof Fourier–Galerkin method exhibits a considerable variation in amplitude as the flow velocity increases beyond

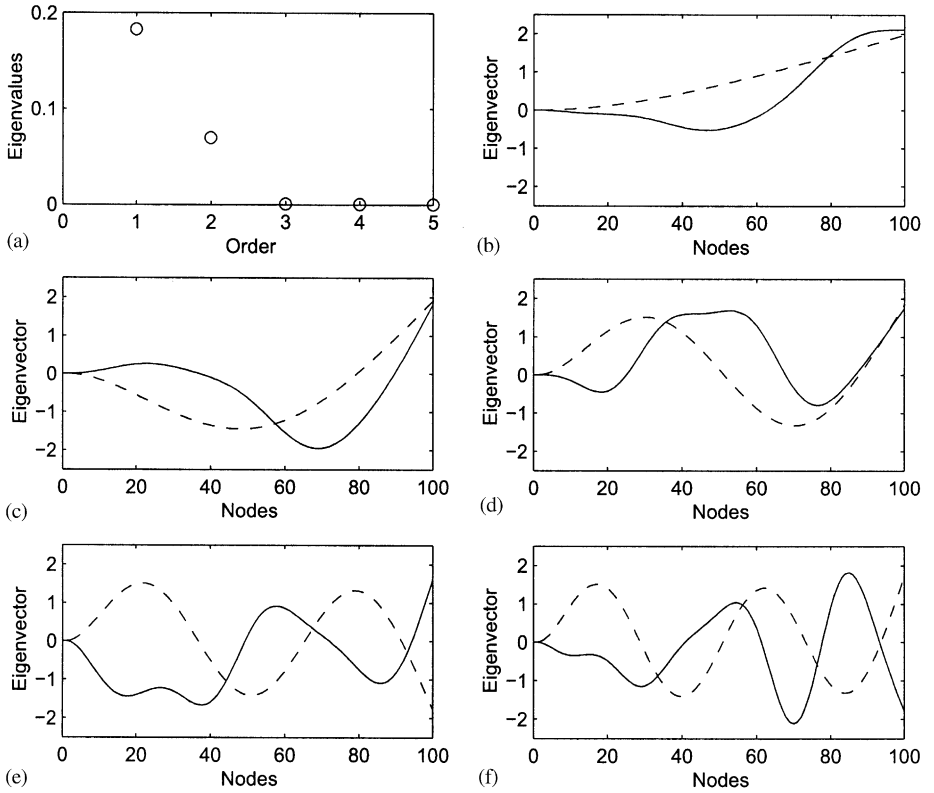

Fig. 10. Eigen-subspace of the weighted correlation matrix for $\gamma = 100$, $\beta = 0.65$ for $u_1 = 20$ and $u_2 = 23$ with corresponding weights $w_1 = 0.5$ and $w_2 = 0.5$: (a) eigenvalue spectrum; (b)–(f) eigenvectors of first to fifth modes (—) compared to corresponding beam mode (- - -).

$u_{cr} = 18$. The bifurcation diagrams using a 4-dof POD-Galerkin method are also plotted, where the POMs having been constructed with the data at flow velocities $u = 20$ and 23. The *weighted* POMs are also constructed with different weights using the time series of the response at $u = 20$ and 23. All these aforementioned POMs are shown in Figs. 8–12. In Fig. 7, the bifurcation diagram using a 4-dof POD-Galerkin scheme are plotted with the corresponding POMs shown in Fig. 10 (with weights $w_1 = w_2 = 0.5$). The bifurcation diagrams obtained using other weighting schemes produce very similar results as will be illustrated later.

The POMs constructed at $u = 20$ and 23 (shown in Figs. 8 and 9) reconstruct the LCO amplitudes with reasonable accuracy in each of the two branches of the bifurcation diagram separated by the flow velocity of $u \simeq 21.8$, as observed in Fig. 7. Unfortunately, POM models which can recreate the result in one branch of the bifurcation diagram display very poor performance in the other branch. Interestingly, the weighted POMs display a far superior performance, identified by its ability to capture the variations in *both* branches of the bifurcation diagram, as also shown in Fig. 7. The reason for the different performance of POMs and weighted POMs will be immediately apparent by examining the POMs in Figs. 8–10. Clearly, the spatial forms of the POMs are considerably different, the differences being more pronounced in the case of the third and fourth POMs. Apparently, the weighted POMs reorient themselves in an optimal fashion to exploit the information from the system response obtained at the two different flow velocities to reconstruct the LCO amplitudes over a broad range of the flow rates. Consequently, a low-dimensional weighted POD model can efficiently represent the original PDE under consideration.

Next, we illustrate the effect of different weighting schemes on the bifurcation diagram constructed using the weighted POD-Galerkin approach. The POMs corresponding to three different weighting schemes are shown in Figs. 10–12. The bifurcation diagrams, obtained using these different weighting schemes, for 2- and 4-dof POD-Galerkin models are shown in Fig. 13(a) and (b), respectively. Although the reduced-order dimension of the POD model is identified by the two largest eigenvalues as shown in Figs. 10–12, a 2-dof POD-Galerkin scheme shows inadequate convergence, as observed in Fig. 13(a). However, the 4-dof POD-Galerkin models obtained using three

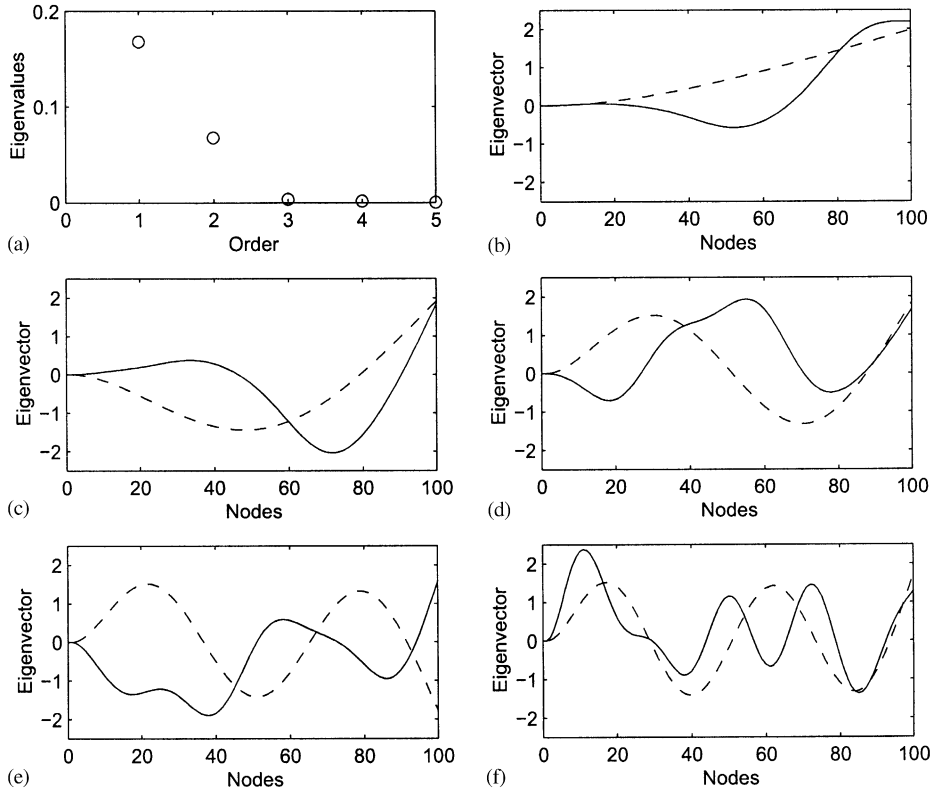

Fig. 11. Eigen-subspace of the weighted correlation matrix for $\gamma = 100$, $\beta = 0.65$ for $u_1 = 20$ and $u_2 = 23$ with corresponding weights $w_1 = 0.95$ and $w_2 = 0.05$: (a) eigenvalue spectrum; (b)–(f) eigenvectors of first to fifth modes (—) compared to corresponding beam mode (- - -).

different weighting schemes exhibit remarkable convergence as clearly shown in Fig. 13(b), irrespective of the weighting used, with the three different curves being nearly identical.

This aspect highlights the importance of the low-energy POMs in higher-dimensional system modelling, as discussed by Lin (1995). It is worthwhile to point out that the weighted POD-Galerkin method appears to be insensitive to the weighting scheme in this specific case. However, the weighted POMs are different, as evident from Figs. 10–12. Seemingly, the POMs obtained using different weighting schemes adapt themselves optimally (depending on the weights) to recreate a reduced model, eventually leading to the same LCO amplitudes, as seen in Fig. 13(b).

Although the results are not presented, the weighted POD-Galerkin models obtained using data from a higher number (more than two) of flow velocities do not appear to improve the results considerably. This means that there is only one significant transition in the POMs, which occurs at a flow velocity of $u \simeq 21.8$ in Fig. 7, with the POMs remaining unchanged within each of the two flow velocity ranges on either side.

5. Concluding remarks

A reduced-order model of the nonlinear PDE describing the dynamics of a hanging cantilever conveying fluid is derived using the well-known proper orthogonal decomposition method. The issues regarding the possibility and suitability of the proper orthogonal modes or *coherent structures* to create a low-dimensional model over a range of flow velocities are addressed. It emerges that the proper orthogonal modes can reconstruct the LCO amplitude with a reduced system over a wide band of flow rates. Furthermore, the superiority of a weighted POD scheme compared to the conventional PODM in order to create a low-dimensional model over a wider range of flow velocity is demonstrated.

The low-dimensional model constructed using the POD-Galerkin approach for nonlinear dynamics and stability analysis can be efficiently used for numerous purposes. The first and foremost advantage of the method is evidently the

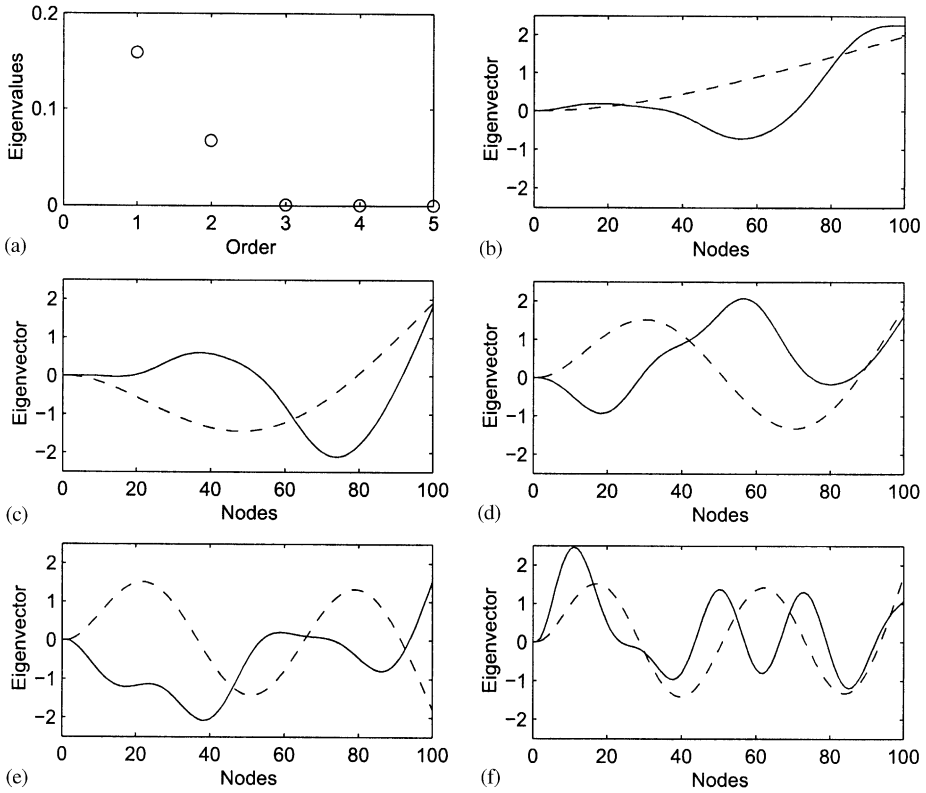

Fig. 12. Eigen-subspace of the weighted correlation matrix for $\gamma = 100$, $\beta = 0.65$ for $u_1 = 20$ and $u_2 = 23$ with corresponding weights $w_1 = 0.05$ and $w_2 = 0.95$: (a) eigenvalue spectrum; (b)–(f) eigenvectors of first to fifth modes (—) compared to corresponding beam mode (- - -).

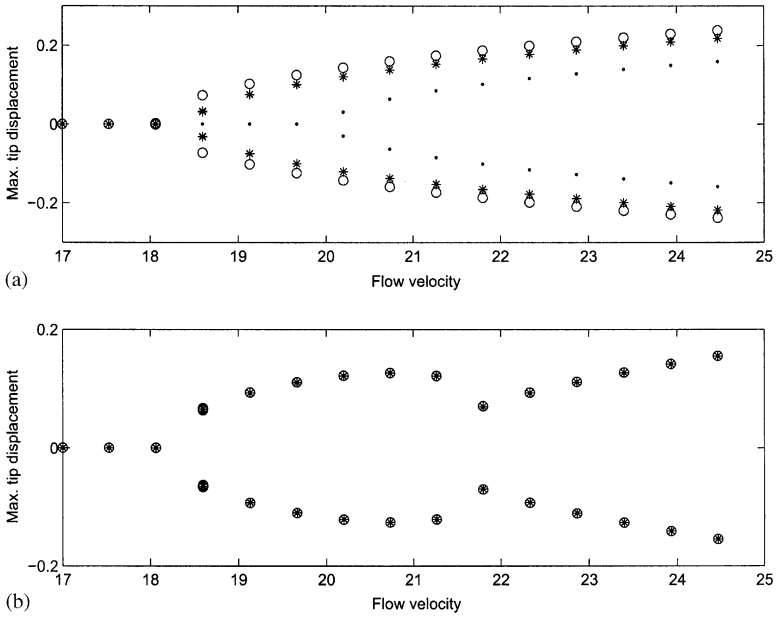

Fig. 13. Bifurcation diagrams obtained with (a) $N = 2$ and (b) $N = 4$ (for $\gamma = 100$ and $\beta = 0.65$) from weighted POD-Galerkin scheme using data at $u_1 = 20$ and $u_2 = 23$ with corresponding weights: $\circ$, $w_1 = 0.95$ and $w_2 = 0.05$; *, $w_1 = 0.5$ and $w_2 = 0.5$; …, $w_1 = 0.05$ and $w_2 = 0.95$.

reduction of the dimensionality of the discretized dynamical system and consequent reduction of computational cost in performing repeated simulations with respect to parameter variations. This is so, for the bifurcation diagrams especially, even when the computational cost of constructing the POMs is factored in. Furthermore, the reduced-order model can conveniently be used to devise an active control strategy.

Presently, the primary emphasis is focussed on the nonlinear dynamics of the *deterministic* PDE describing the motion of the cantilever pipe conveying fluids. However, when the flow is subjected to random fluctuations, the dynamic motion of the pipe is governed by a *stochastic* differential equation. Reduced-order modelling can be immensely advantageous in investigating the behaviour of such a *stochastic* PDE.

Acknowledgements

The first author gratefully acknowledges the financial support of a NSERC Postdoctoral Fellowship to carry out this research. The authors appreciate interesting discussions with Dr Christian Semler, especially in the matters pertaining to the numerical computations, by making certain computer codes available.

References

Aubry, N., Holmes, P., Lumley, J.L., Stone, E., 1988. The dynamics of coherent structures in the wall region of a turbulent boundary layer. Journal of Fluid Mechanics 192, 115–173.

Berkooz, G., Holmes, P., Lumley, J.L., 1993. The proper orthogonal decomposition in the analysis of turbulent flows. Annual Review of Fluid Mechanics 25, 539–575.

Breuer, K.S., Sirovich, L., 1991. The use of the Karhunen–Loéve procedure for the calculation of linear eigenfunctions. Journal of Computational Physics 96, 277–296.

Christensen, E.A., Brons, M., Sorensen, J.N., 2000. Evaluation of proper orthogonal decomposition techniques applied to parameter-dependent nonturbulent flows. SIAM Journal of Scientific Computing 21, 1419–1434.

Cusumano, J.P., Bai, B.Y., 1993. Period-infinity periodic motions, chaos, and spatial coherence in a 10 degree of freedom impact oscillator. Chaos, Solitons & Fractals 3, 515–535.

Das, I., Dennis, J.E., 1997. A closer look at drawbacks of minimizing weighted-sums of objectives for Pareto set generation in multicriteria optimization problems. Structural Optimization 14, 63–69.

Dowell, E.H., Hall, K.C., Romanoski, M.C., 1997. Eigenmode analysis in unsteady aerodynamics: reduced order models. Applied Mechanics Review 50, 371–386.

Georgiou, I.T., Schwartz, I., Emaci, E., Vakakis, A., 1999. Interaction between slow and fast oscillations in an infinite degree-of-freedom linear system coupled to a nonlinear subsystem: theory and experiment. Journal of Applied Mechanics 66, 448–459.

Hall, K.C., Thomas, J.P., Dowell, E.H., 2000. Proper orthogonal decomposition technique for transonic unsteady aerodynamic flows. AIAA Journal 38, 1853–1862.

Kim, T., 1998. Frequency-domain Karhunen–Loeve method and its application to linear dynamic systems. AIAA Journal 36, 2117–2123.

Kim, T., 2001. An efficient response-based modal analysis for dynamic systems with multiple inputs. 42nd AIAA/ASME/ASCE/ASC Structures, Structural Dynamics, and Materials Conference, AIAA-2001-1380.

Kim, T., Bussoletti, J.E., 2001. An optimal reduced-order aeroelastic modeling based on a response-based modal analysis of unsteady CFD models. 42nd AIAA/ASME/ASCE/ASC Structures, Structural Dynamics, and Materials Conference, AIAA Paper-2001-1525.

Kim, T., Nagaraja, K.S., Bhatia, K.G., 2001. Application of FDKL method for order reduction of RFA unsteady aeroelasticity models. 42nd AIAA/ASME/ASCE/ASC Structures, Structural Dynamics, and Materials Conference, AIAA Paper-2001-1524.

Koski, J., 1985. Defectiveness of weighted method in multicriteria optimization of structures. Communications in Applied Numerical Methods 1, 333–337.

Kreuzer, E., Kust, O., 1996. Proper orthogonal decomposition—an efficient means of controlling self-excited vibrations of long torsional strings. In: Bajaj, A.K., et al. (Eds.), Nonlinear Dynamics and Controls, DE-Vol. 91. ASME, New York, pp. 105–110.

Kwasniok, F., 1997. Optimal Galerkin approximation of partial differential equations using principal interaction patterns. Physical Review E 55, 5363–5375.

Kwasniok, F., 2001. Low-dimensional models of the Ginzburg-Landau equation. SIAM Journal of Applied Mathematics 61, 2063–2079.

Lenaerts, V., Kerschen, G., Golinval, J.C., 2001. Proper orthogonal decomposition for model updating of non-linear mechanical systems. Mechanical Systems and Signal Processing 15 (1), 31–43.

Lin, D.C., 1995. Characterization of low-energy mode vibrations in chaos using entropy balance versus the amplitude-based Karhunen–Loeve expansion. Physical Review E 52, 2322–2329.

Loève, M., 1977. Probability Theory, 4th Edition. Springer, New York.

Ma, X., Vakakis, A.F., 2001. Nonlinear transient localization and beat phenomena due to backlash in a coupled flexible systems. ASME Journal of Vibration and Acoustics 123, 36–44.

Ma, X., Azeez, M.F.A., Vakakis, A.F., 2000. Non-linear normal modes and non-parametric system identification of non-linear oscillators. Mechanical Systems and Signal Processing 14, 37–48.

Païdoussis, M.P., 1970. Dynamics of tubular cantilevers conveying fluid. Journal of Mechanical Engineering Science 12, 85–103.

Païdoussis, M.P., 1998. Fluid–structure Interactions: Slender Structures and Axial Flow. Academic Press, London.

Païdoussis, M.P., Li, G.X., 1993. Pipes conveying fluid: a model dynamical problem. Journal of Fluids and Structures 7, 137–204.

Païdoussis, M.P., Semler, C., 1993. Nonlinear and chaotic oscillations of a constrained cantilevered pipe conveying fluid: a full nonlinear analysis. Nonlinear Dynamics 4, 655–670.

Païdoussis, M.P., Semler, C., 1998. Non-linear dynamics of a fluid-conveying cantilevered pipe with a small mass attached at the free end. International Journal of Non-linear Mechanics 33, 15–32.

Pareto, V., 1906. Societa Editrice Libraria. (Translated into English by A.S. Schwier as Manual of Political Economy, MacMillan, New York, 1971).

Park, H.M., Cho, D.H., 1996. The use of Karhunen–Loeve decomposition for the modeling of distributed parameter systems. Chemical Engineering Science 51, 81–98.

Park, H.M., Lee, M.W., 2000. Control of Navier–Stokes equations by means of mode reduction. International Journal for Numerical methods in Fluids 33, 535–557.

Park, H.M., Yim, O.Y., 1998. A reduction method for the boundary control of the heat conduction equation. Journal of Dynamic Systems, Measurement, and Control 122, 435–444.

Sarkar, A., Ghanem, R., 2001. Mid-frequency structural dynamics with parameter uncertainty. 42nd AIAA/ASME/ASCE/ASC Structures, Structural Dynamics, and Materials Conference, AIAA Paper-2001-1454.

Semler, C., Païdoussis, M.P., 1995. Intermittency route to chaos of a cantilevered pipe conveying fluid with a mass defect at the free end. Journal of Applied Mechanics 62, 903–907.

Semler, C., Li, G.X., Païdoussis, M.P., 1994. The non-linear equations of motion of pipes conveying fluid. Journal of Sound and Vibration 169, 577–599.

Semler, C., Gentleman, W.C., Païdoussis, M.P., 1996. Numerical solutions of second order implicit non-linear ordinary differential equations. Journal of Sound and Vibration 195, 553–574.

Sirovich, L., 1987a. Turbulence and dynamics of coherent structures, Part I: coherent structures. Quarterly of Applied Mathematics 45, 561–571.

Sirovich, L., 1987b. Turbulence and dynamics of coherent structures, Part II: symmetries and transformations. Quarterly of Applied Mathematics 45, 573–582.

Sirovich, L., 1987c. Turbulence and dynamics of coherent structures, Part III: dynamics and scaling. Quarterly of Applied Mathematics 45, 583–590.

Sirovich, L., 1989. Chaotic dynamics of coherent structures. Physica D 37, 126–145.

Sirovich, L., Deane, A.E., 1991. A computational study of Rayleigh–Benard convection. Part 2. Dimension considerations. Journal of Fluid Mechanics 222, 251–265.

Sirovich, L., Rodriguez, J.D., 1978. Coherent structures and chaos: a model problem. Physical Review Letters A 120, 211–214.

Sirovich, L., Knight, B.W., Rodriguez, J.D., 1990. Optimal low-dimensional dynamical approximations. Quarterly of Applied Mathematics 48, 535–548.

Thomas, J.P., Dowell, E.H., Hall, K.C., 2001. Three-dimensional transonic aeroelasticity using proper orthogonal decomposition based reduced order models. 42nd AIAA/ASME/ASCE/ASC Structures, Structural Dynamics, and Materials Conference, AIAA Paper-2001-1526.

Zlobec, S., 2001. Stable Parametric Programming. Kluwer Academic Publishers, Dordrecht.